Geological Quarterly, 2024, 68: 22
DOI: http://dx.doi.org/10.7306/gq.1750

ERT field survey supported with numerical and analogue modeling applied to study a fragment of the Pieniny Klippen Belt (Spisz Pieniny Mountains, southern Poland)

Grzegorz BANIA[1,] *, Włodzimierz Jerzy MOŚCICKI[1] and Jan GOLONKA[1]

[1] AGH University of Krakow, Faculty of Geology, Geophysics and Environmental Protection, al. A. Mickiewicza 30, 30-059; ORCID: 0000-0002-9661-8184 [G.B.], 0000-0003-3593-9192 [W.J.M.], 0000-0001-9671-5809 [J.G.]

Bania, G., Mościcki, W.J., Golonka, J., 2004. ERT field survey supported with numerical and analogue modeling applied to study a fragment of the Pieniny Klippen Belt (Spisz Pieniny Mountains, southern Poland). Geological Quarterly, 2024, 68: 22; http://doi.org/10.7306/gq.1750

Associate editor: Piotr Krzywiec

Electrical Resistivity Tomography (ERT) method was applied to study a fragment of the Pieniny Klippen Belt (PKB), which has been investigated for more than 100 years. The study area is located in the Spisz Pieniny Mountains of southern Poland. The PKB in this region includes a characteristic belt of limestone outcrops. ERT turned out to be an effective method to determine the structure of this part of the PKB, revealing its zonal nature and documenting the presence of limestone olistoliths and allowing estimates of their sizes. Moreover, we show that proper planning and conducting of ERT measurements in the field is critical to the effective use of resistivity data for geological inference and interpretation. This has been demonstrated by performing appropriate numerical and analogue ERT modeling that shows possible ambiguous results arising from the field ERT survey. Awareness of this issue can help researchers avoid and minimize false interpretation of ERT data.

Key words: Pieniny Klippen Belt, olistoliths, mélange, electrical resistivity tomography (ERT), ERT modeling, inversion ambiguity.

INTRODUCTION

Electrical Resistivity Tomography (also called Electrical Resistivity Imaging – ERI; Dahlin, 1996) is a widely used geophysical Direct Current (DC)-resistivity method. It enables the recognition of the two- and three-dimensional (2D/3D) distribution of electrical resistivity in geological environment. It is commonly applied in geological and geomorphological research (see, e.g., Hirsch et al., 2008; Šilhán and Pánek, 2010; Chambers et al., 2012; Ikhane et al., 2012; Metwaly and AlFouzan, 2013; Mościcki et al., 2014; Nur Amalina et al., 2017; Woźniak et al., 2018; Akinbiyi et al., 2019; Woźniak and Bania, 2019a, b; Bania and Woźniak, 2022), as well as in other studies (see, e.g., Loke et al., 2013 and references therein).

Most often, the ERT method is performed in the 2D mode (understood as measurements along a single straight line with results processed and interpreted with the use of 2D software). It is a very effective method, but its correct use and especially its proper interpretation require experience, geophysical knowledge, and an appropriate approach. We describe the application of ERT to the study of part of the Pieniny Klippen Belt (PKB), which has more than 100 years of study (Golonka et al., 2022). This ERT survey sought to determine the distribution of electrical resistivity in this rock unit and, in this way, to recognize the structure of this segment of the PKB. Questions of interest concerned the spatial extent of the limestone, flysch, marl and clay/shale components, and the size and mutual arrangement of the limestone blocks (olistoliths).

In addition to solving geological problems, the results of our study demonstrated the importance of further interpretation in properly planning and executing 2D ERT fieldwork. Failure to properly apply 2D inversion to ERT data may lead to erroneous geophysical/geological conclusions, as shown by the results of our field studies and of the associated analogue and numerical modeling of the ERT data.

RESEARCH AREA

The study area (Fig. 1) is located in the Spisz Pieniny Mts. region in southern Poland. The Central Carpathians and the Pieniny Klippen Belt (PKB) occur in this region (Birkenmajer, 2017; Golonka et al., 2022). The general geological situation is shown in Figure 2A. The recently published map (Cichotępski et al., 2024) includes previous studies by Birkenmajer (1961,

* Corresponding author, e-mail: bania@agh.edu.pl
Received: October 3, 2023; accepted: May 2, 2024; first published online: 18 July, 2024

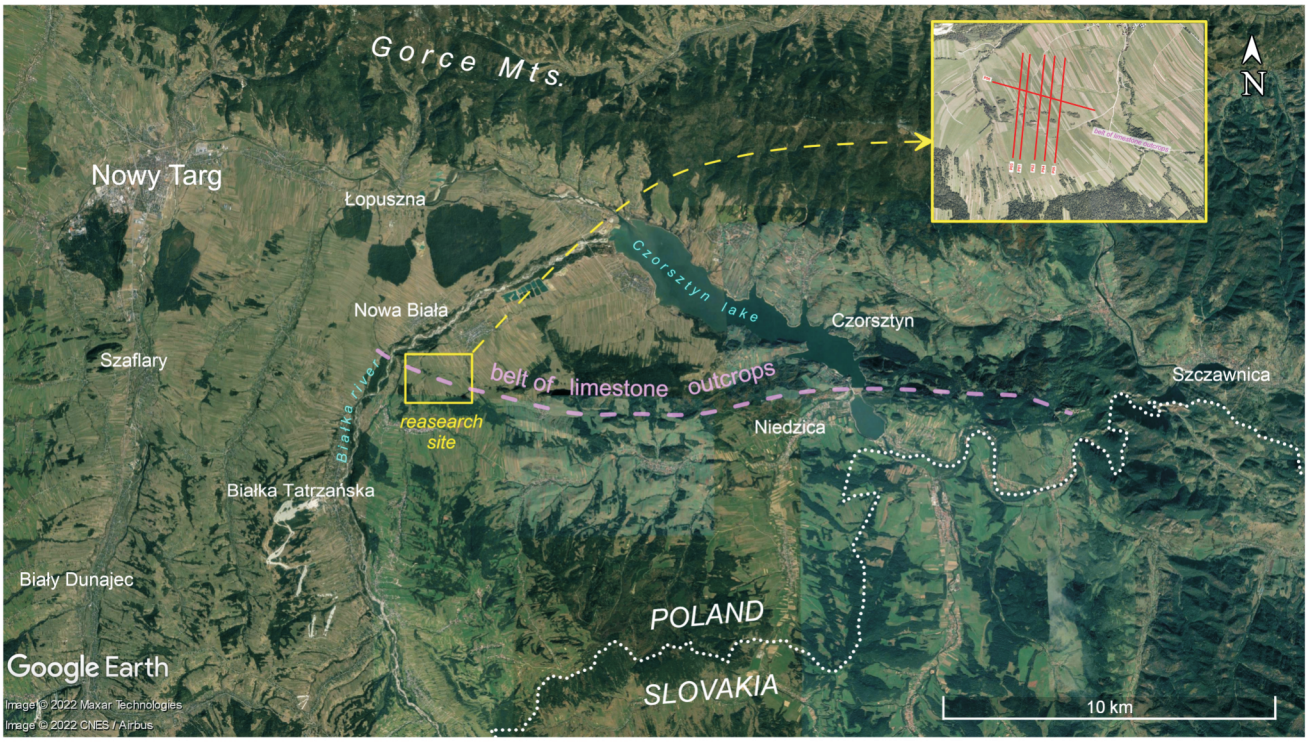

Fig. 1. Location of the study area

ERT survey marked with red lines (source of orthophotomap: Google Earth)

1977, 1979, 2017), Watycha (1964, 1975) and results of the latest geological mapping.

The Central Carpathian rocks crop out in the southernmost part of the area investigated. They are represented by flysch deposits of the Central Carpathian Paleogene (Podhale Flysch) and (mainly) by Eocene sandstone and shales of the Szaflary Formation (Ludwiniak, 2010; Golonka et al., 2019). A subvertical fault marks the boundary between the Central Carpathian Paleogene and PKB (Birkenmajer, 2017; Golonka et al., 2022). The Central Carpathian Paleogene flysch rocks are strongly deformed and dip steeply, almost vertically, near this boundary, and gently a few kilometres south of the PKB (Golonka et al., 2019, 2022).

The PKB is a tectonic unit that constitutes a 600 km-long suture zone (Andrusov, 1965; Książkiewicz, 1977; Birkenmajer, 2017; Plašienka et al., 2021; Golonka et al., 2022) between the ALCAPA (Alpine–Pannonian–Carpathians) (Csontos and Vörös, 2004) and the North European Plate covered by overthrusted Outer Carpathian units. The name Pieniny Klippen Belt (Pieninische Klippenzug) was first used by Neumayr (1871) and relates to this mountain range in Poland, which is made of the western Spisz (Spiš) Pieniny Mts., the central Pieniny Mts. and the eastern Małe (Little) Pieniny Mts. (Kondracki, 2001).

The PKB name also reflects the relatively erosion-resistant blocks named Klippen (cliffs), that stand out from within less competent flysch units (Golonka et al., 2019, 2022; Plašienka et al., 2021). The Polish part of the PKB (Fig. 2A) has been studied by geologists since the 19th century. These studies described traditional stratigraphic successions, named after localities in the Polish part of the PKB (Birkenmajer, 1977, 2017), and differentiated mainly on the basis of the Jurassic–Cretaceous rocks that form the klippen. They are also classified based on their palaeographic position within the ridge, slope, and deeper basin. Some of the klippen are olistoliths, i.e., homogeneous or heterogeneous rock blocks of various sizes that were moved by gravity downslope towards the flysch basins (Golonka et al., 2015). Other klippen became juxtaposed with the flysch as a result of tectonic deformation that occurred during orogenic movements (Birkenmajer, 2017; Plašienka et al., 2021).

The PKB rocks were deposited during Jurassic-Neogene times in the Alpine Tethys within two basins, Złatne and Magura, divided by the Czorsztyn Ridge (Sikora, 1971; Golonka et al., 2019, 2022). The Hulina successions were deposited on the northern slope of the Czorsztyn Ridge (Golonka et al., 2022), the name Hulina being introduced by Sikora (1971). Later, the name Grajcarek has also been used (e.g., Birkenmajer, 1977, 2017). The Czorsztyn Succession was deposited on the central part of this ridge. The Pieniny, Branisko, Czertezik and Niedzica successions were deposited on the southern slope of this ridge. The Złatne Succession was deposited in the central part of the Złatne Basin (Golonka et al., 2022). The Jurassic–Lower Cretaceous deposits are mainly represented by limestones and radiolarites (Birkenmajer, 1977, 2017). They form klippen belonging to tectonic units emplaced within the surrounding clastic deposits by compressional processes or to olistoliths that slid down from elevated ridge areas into deeper basinal zones (Golonka et al., 2015, 2022). The rocks of the Czorsztyn Succession exposed in the research area comprise olistoliths redeposited into a mélange. Albian-Neogene rocks are represented mainly by flysch and marls that were deposited as an accretionary prism formed (Birkenmajer, 1977, 2017; Golonka et al., 2022).

The present-day structure of the PKB is a result of compressional and transpressional movements (Golonka et al.,

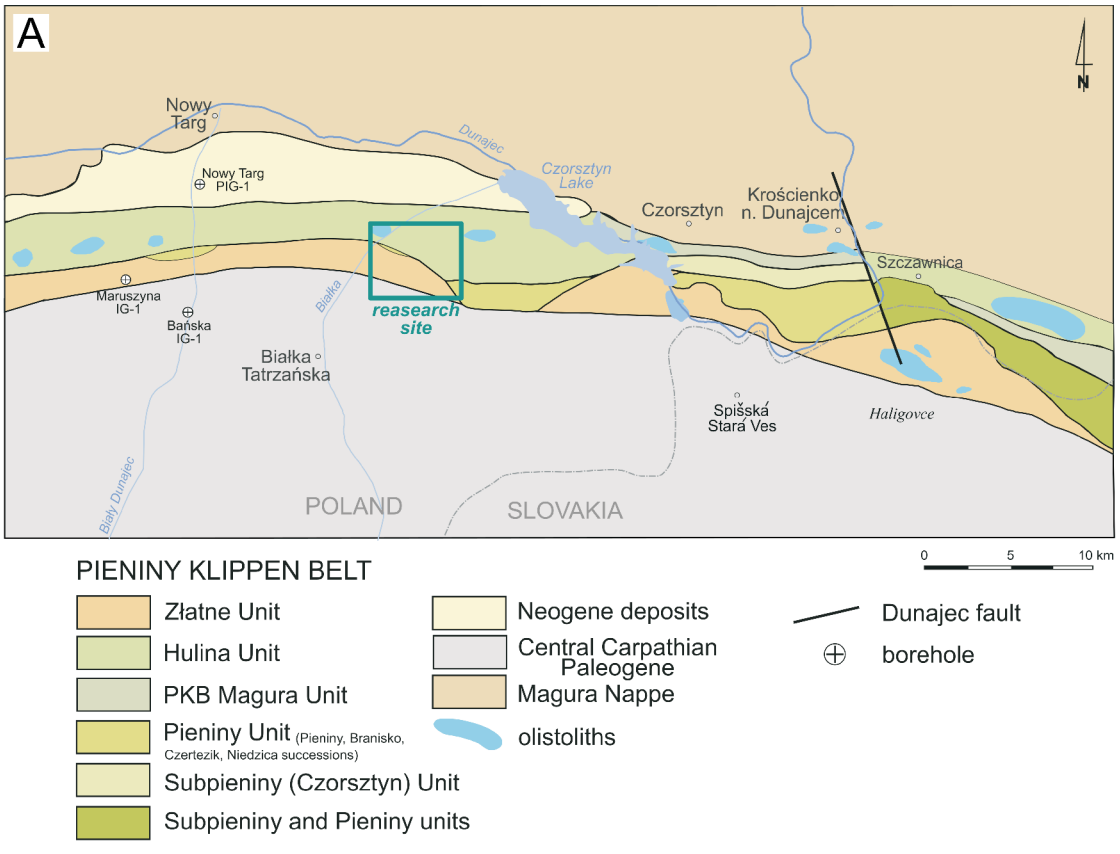

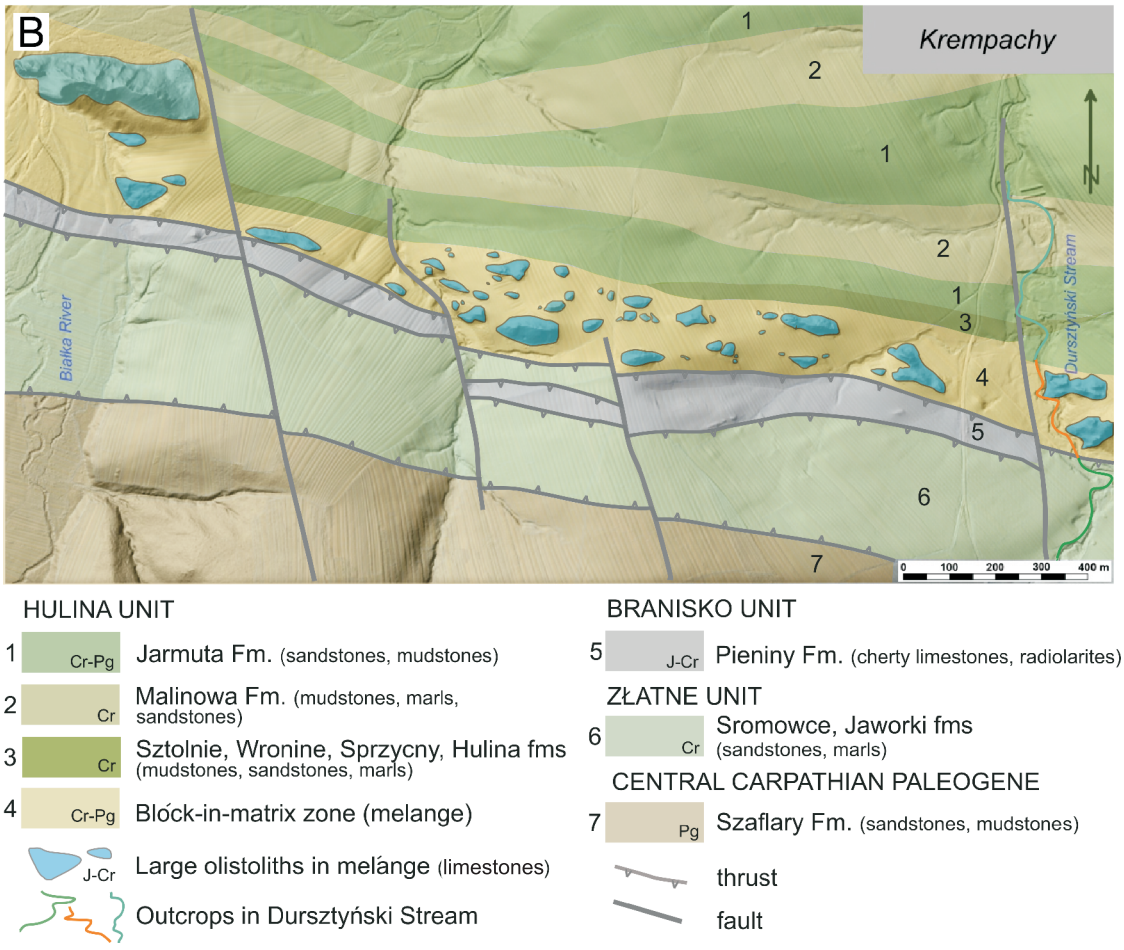

Fig. 2. Geological maps

A – sketch map of the Pieniny Klippen Belt in Poland (after Golonka et al., 2018, modified) and location of the geophysical research site; **B** – geological map of the study area superimposed on the DEM image (with 1 m cell size; source: www.geoportal.gov.pl; after Cichostępski et al., 2024, modified)

2019, 2022). Compressional deformation produced thrust-sheets (nappes). Three tectonic units (nappes) have been distinguished within the area investigated: Złatne, Branisko, and Hulina units (Fig. 2B). The southern Złatne Unit is located north of the Central Carpathian Paleogene flysch. It comprises mainly Upper Cretaceous flysch of the Sromowce Formation (Golonka et al., 2019, 2022). The northern Hulina Unit is built mainly of Upper Cretaceous-Paleocene flysch of the Jarmuta and Malinowa formations (Sikora, 1971; Birkenmajer, 2017; Golonka et al., 2019, 2022). Components with prevailing thick-bedded massive sandstones, or with an equal mixture of shales and sandstones, can be distinguished within this flysch. In addition, a block-in-matrix zone with olistoliths representing a sedimentary mélange can be distinguished within the Hulina Unit north of the boundary with Złatne Unit. This zone corresponds to a belt of limestone outcrops, with olistoliths mainly composed of Jurassic-Cretaceous limestones belonging to the Czorsztyn Succession. They are often arranged vertically, contrasting with the 45° dip of the flysch nappes (Golonka et al., 2019). The Branisko Unit consists mainly of Jurassic–Lower Cretaceous pelagic limestones and radiolarites of the Branisko Succession (Birkenmajer, 1977, 2017; Golonka et al., 2022). The type area of this succession is located on Branisko Mt. within the Spisz Pieniny Mts. (Birkenmajer, 1977). The Branisko Unit crops out only locally in the research area (Fig. 2B).

The thrusts of the Złatne, Pieniny, and Hulina units represent a tectonic mélange. This mixture of sedimentary and tectonic mélange characterizes the PKB in the Spisz Pieniny Mts., being a result of Cretaceous-Miocene folding, tectonic movement, and uplift. The overriding of the Czorsztyn ridge by an accretionary prism contributed to the formation of a sedimentary mélange within the Hulina Unit, containing carbonates of the Czorsztyn Succession (Golonka et al., 2022).

METHODS

SOME REMARKS ON THE ERT METHOD

In our study, ERT method was applied in two-dimensional (2D) mode, as measurements along a single straight line. Technically, such a 2D ERT survey consists of placing several tens (or even hundreds) of electrodes along a straight survey line, usually at equal distances (spacing – Δx) and performing DC-resistivity profiling (Telford et al., 1990) with many different arrays (the array consists of four selected electrodes). Appropriate selection of the spacing as well as the type, amount, and size of the arrays allows one to investigate the medium with the planned detail and the desired depth of investigation. As a result, a set of apparent resistivity (not true resistivity) values for different arrays and for different positions of the array on the profile is obtained. The field data set is shown as a two-dimensional Apparent Resistivity Pseudosection (ARP) with the pseudodepth (a quantity which depends on the size and type of array) in the vertical direction, and the position of the array on the survey line in the horizontal direction. The ARP is then interpreted quantitatively, via inversion (e.g., Loke, 2012). The aim of the inversion is to "convert" the apparent resistivity pseudosection into a section showing the distribution of true resistivity (understood as a physical property) as a function of the actual depth. This is achieved through the iterative selection of such a theoretical (numerical, blocky) 2D true resistivity distribution model so that the simulated (i.e., theoretical – numerically calculated) measurements on it are as close as possible to the results of field measurements. For this, the measured ARP is compared with the theoretical (i.e. calculated) one. If they do not match, the proposed numerical model is corrected, and the fitting procedure is reiterated. The model is assumed to be correct if both sections are acceptably similar. A measure of this correctness is the theoretical-to-field ARP fitting error (depending on the inversion method applied, it may be an RMS or Absolute Error). Formally, the lower the error value, the better (Loke, 2012). As a result of multiple repetitions (iterations) of the process of improving the proposed model, the final result is a cross-section of a specific 2D resistivity distribution in the axis system: Z – depth, X – distance along the survey line. This is not an actual (real property) resistivity section but an inverse (theoretical) 2D model resistivity section (i.e. an inversion model). Furthermore, the inversion is inherently ambiguous (as, in this case, mathematically it is an "ill-posed problem": Kabanikhin, 2008). This means that even for an ideal 2D situation and negligible measurement errors, there are many possible and equivalent interpretation models (a practical example of ERT inversion ambiguity is given in, e.g., Bania and Ćwiklik, 2013). For better interpretation and understanding of the specificity of ERT results, analogue modeling can sometimes provide good support (e.g., Mościcki, 2008; Bania and Ćwiklik, 2013; Woźniak and Bania, 2019a; Szalai et al., 2020; Hojat et al., 2021).

The result of the formal inversion also depends on the numerical approach/solution used in the software, and the results for the same data set may differ (e.g., Hellman et al., 2016) which further complicates the final interpretation. Moreover, results of ERT survey/inversion may also depend on the applied set (size, type, and number) of arrays (Dahlin and Zhou, 2004).

A further important question is to what extent the measurement conditions (subsurface geology, usually only poorly predicted, and simultaneously known and measurable terrain morphology) influence the result of the 2D inversion of the ERT data.

The 2D mode of inversion is commonly applied, although the measurements taken may not comply with the relevant 2D criteria (described in Section: Analysis of the P06 profile results – notes on the correct application of the 2D ERT method). This may lead to serious interpretation errors. Nevertheless, this problem is commonly not taken into account.

Even if low-error inversion results are obtained, an additional crucial but difficult task is to choose a solution that has the most probable geological sense. For that, the resistivity cross-section obtained from the inversion (and its variants) should be further analysed, with the use of all possible information or data (geological, geotechnical, borehole, environmental, etc.) to finally propose an acceptable (though still only probable) model. Unfortunately, in the case of the PKB segment in our geophysical survey area (and up to several kilometres away), few surface geological observations are available, and no borehole data.

DATA ACQUISITION AND PROCESSING

2D ERT FIELD MEASUREMENTS

The ERT survey was carried out on a small area of the PKB (Fig. 1). Most of the 2D ERT measurements were carried out along a survey lines oriented perpendicular to the belt of limestone outcrops, here a clearly visible part of the PKB (Fig. 3).

The 2D ERT measurements were conducted using *SuperSting R8/IP/SP* apparatus (manufactured by Advanced Geosciences, Inc., AGI) with the use of 112 electrodes placed with a spacing of $\Delta x = 5$ m. The predefined pattern of the measurement procedure (i.e., the sequence of changes of the ar-

rays and the order of measurements with these arrays) was prepared to achieve desirable resolution and depth of investigation. To make most of the *SuperSting 8-channel* measurement method, the Multiple Gradient Array was applied (GD; Dahlin and Zhou, 2004).

For every array, the relations between the lengths of current dipole AB and potential dipole MN were held the same, that is, MN = 0.1 AB. The applied current AB dipoles were: 50, 100, 150, 200, 250, 300, 350, 400, 450, 500, and 550 m. For the shallowest penetration depth, Wenner array: A-5-M-5-N-5-B, and dipole-dipole arrays: M-15-N-*n* × 15-A-15-B (*n* = 1, 2, 3, 4, 5) were additionally used.

The initial part of each survey line was 555 m long. By applying the roll-along technique (Dahlin, 2001; Loke, 2012), measurements were continued for the rest of the planned survey line, ~1 km length in all cases. There were no technical problems while performing the resistivity measurements. The grounding resistance of all electrodes was low, as clayey soil covered by meadow vegetation dominates in that area (Fig. 3A–F).

The amount of data recorded for the individual survey line exceeded 12,000 values of apparent resistivity. Data measured varies between profiles due to different measurement errors. Additional information for all survey lines is given in Table 1.

For proper inversion of the field ERT data, the morphology of the survey line needs to be known (Fox et al., 1980; Loke, 2000; Lu et al., 2015). The topography of all ERT profiles was obtained on the basis of a high-resolution digital elevation model (DEM), that is, a rectangular mesh with a mesh size of 1 x 1 m (source: www.geoportal.gov.pl). Selected segments of ERT survey lines were also measured and leveled using a GNSS receiver operating in RTK-RTN mode. The differences in the accuracy of the relief mapping turned out to be very small and fully acceptable from a geophysical point of view, considering the scale of the study.

The geophysical survey was supplemented by geological mapping. This mapping was conducted mainly along the streams and in the block-in-matrix zone with olistoliths.

ERT DATA INVERSION

Res2Dinvx64 software (ver. 4.06.16; *Geotomo software*; Loke, 2012) was used to invert the ERT data. It enables the performing of two different inversion procedures, i.e., L1-norm (robust, blocky) and L2-norm (smooth) (Loke et al., 2003). According to the geological information on the PKB (Golonka et al., 2022), the rocks analysed have the character of very distinct vertical structures with sharp boundaries. It can be assumed that in such cases the use of robust inversion will bring better results (e.g., Dahlin and Zhou, 2004; Danielsen and Dahlin, 2010; Woźniak and Bania, 2019a). This was also tested by Bania and Ćwiklik (2013) using analytical modeling in *Res2Dmod* software. It follows that the reproduction of sharp-edged structures with high resistivity contrast is much better for blocky inversion. For all ERT data, the L1-norm inversion mode, with some modifications of default settings, was then applied. After the first run of the inversion, the results obtained were analysed and data with individual fitting errors (described earlier) exceeding 20% were rejected (Table 1). Then the final inversion run of the corrected data was performed. Final 2D sections were prepared with the use of *SURFER* software (Golden Software).

ERT ANALOGUE MODELING

Analogue modeling was performed at the Geoelectrical Laboratory (Department of Geophysics; Faculty of Geology, Geophysics and Environmental Protection, at the AGH University of Krakow). For analogue geoelectrical studies, a special tank was constructed that can be filled with water (Fig. 4A). Along its longer axis, there is a system of 100 brass electrodes mounted on a Plexiglas plate every 1.5 cm that simulates the ERT survey line (Fig. 4B). The set of cables connects the electrodes to the measuring equipment, SuperSting or MiniSting (Advanced Geosciences, Inc., AGI). Depending on the purpose of the planned experiment, one or more anomalous objects of arbitrary shape, size, and position may be mounted below or near the measuring line (Fig. 4C). For practical reasons, the objects (models) are mostly electrical insulators.

One of the problems encountered in small-scale laboratory measurements are errors connected with unavoidable inaccuracies in electrode size and arrangement, limited tank dimensions, and other factors. To limit these errors, resistivity measurements are usually performed at least twice. First, the "background" or "normal field" (N) is measured for the tank filled with water, but without the immersed model. Next, after immersion of the anomalous model/body, the measurements are repeated to obtain the apparent resistivity image – anomaly (A). Then, A/N normalization is performed to reduce (limit) the possible influence of the previously mentioned inaccuracies on the resistivity measurements.

During ERT laboratory measurements, the same pattern of the measurement procedure, that is, a multiple gradient array as for the field survey (array dimensions were properly downscaled), was applied.

A physical model of a "wall" as considered in this study is shown in Figure 4D. Sketches of the actual models, both numerical and analogue, are provided in the Discussion Section, (see Fig. 9).

2D ERT NUMERICAL MODELING

For numerical modeling, *Res2Dmod* software (ver. 3.03.06; *Geotomo* software; Loke, 2012) was used. The same pattern (GD array) of the measurements as for analogue modeling was applied.

NOTES ON GEOLOGICAL INTERPRETATION OF THE ERT INVERSION RESULTS

Knowledge of the resistivity-lithology relationship is essential for making geological use of the results of geophysical interpretation (inversion).

There is no unambiguous relationship between resistivity and lithology. This is because the *in situ* resistivity of a rock is influenced by various factors (e.g., Keller and Frischknecht, 1966; McNeill, 1980; Kobranova, 1989; Telford et al., 1990): lithological type, texture, water content, degree of fracturing, weathering, conditions of occurrence, and others. In the case of porous rocks, the nature of the pores and the degree of filling with water or air have a particularly large influence on the electrical resistivity. This also applies to cracked, fractured and weathered rocks. Generally, the presence of water reduces the resis-

Fig. 3. Field views of the research site

A – location of the P06 survey line, Czerwona Skałka is in the background; **B** – measurements on the P06 profile with the *SuperSting* resistivity system; **C** – general view of the P02 survey line crossing the BoLO; **D** – location of the P01 survey line, Kramnica is in the background; **E** – preparation of the P03 profile for measurements; **F** – view of the beginning of the P01 profile; the BoLO is visible in the middle part of the photo; the Gorce Mountains are visible in the background; **G** – view of part of the Lorencowe Skałki with its most striking part, Gęśle; they are located close to the research site, in the east; **H** – general view of the southern part of the research site with the Tatra Mountains visible in the background

Table 1

Characteristics of field measurements and robust inversion (Res2Dinvx64) results for the ERT method

ERT survey line name	Number of data collected	Number of data after filtration	Number of inversion iterations	Inversion absolute error [%]
P01	12086	12086	10	0.76
P02	12066	11194		1.67
P03	12074	11158		1.57
P04	12085	11812		1.25
P05	12044	11035		1.93
P06	11966	11504		0.95

For each survey line, the effective number of electrodes (regarding roll-along overlaps) was 196 and the spacing, Δx = 5 m

Fig. 4. Analogue modeling setup

A – fibreglass tank; **B** – (1), (2) – holders for hanging the plate with electrodes and for models; (3) – plexiglas plate with electrodes – survey line; M1 and M2 – examples of anomalous objects (models); **C** – line of electrodes (4) seen from below; **D** – tank and model of the "wall" prepared for measurements

tivity, while air (gas) increases it. The chemical properties of the water (salinity) determine the scale of its impact on the resistivity of the rock medium. Saline water significantly reduces resistivity depending on the salt concentration (Dortman, 1992).

Information about the true resistivity of rocks is most often obtained by laboratory measurements. However, sample sizes are limited (although often they are standardized), but a more important issue is their proper representativeness. Neverthe-

less, the measured resistivity refers directly to a physical property and usually does not need further special interpretation. On the other hand, in-field geophysical DC-resistivity measurements, using ERT and VES (Vertical Electrical Sounding) methods, give simplified, spatially averaged information about the resistivity distribution in the geological medium. In this case, the "sample" size is unlimited and, additionally, the sample may be (and usually is) heterogeneous. The measurement result (apparent resistivity, not true resistivity) depends on the type, size, and layout of the measuring array. To estimate the distribution of the rock resistivity values, a special quantitative interpretation (inversion) of the measurement data is needed. The values obtained in this way usually differ from the resistivity values of the rock samples determined in the laboratory, and various rock types may have similar or overlapping ranges of possible resistivity values, hampering the geological interpretation of DC-resistivity surveys.

The many DC-resistivity field surveys performed in Poland (e.g., Antoniuk et al., 2005; Woźniak et al., 2018; Woźniak and Bania, 2019a; Bania and Woźniak, 2022) suggest the following general patterns: in flysch, the rock resistivity depends on the proportion of sandstone (high resistivity) to shale (low resistivity). Relatively clean clay rocks most often have a resistivity of <10–15 m (and for those of marine origin it can drop to a few m); for sandstones, depending on the type, several hundred to a thousand Wm (even more in the case of quartzite); for clean, compact limestone, several hundred or more Wm; for marly limestones, several tens of Wm. Thus, the value is determined mostly by the clay component.

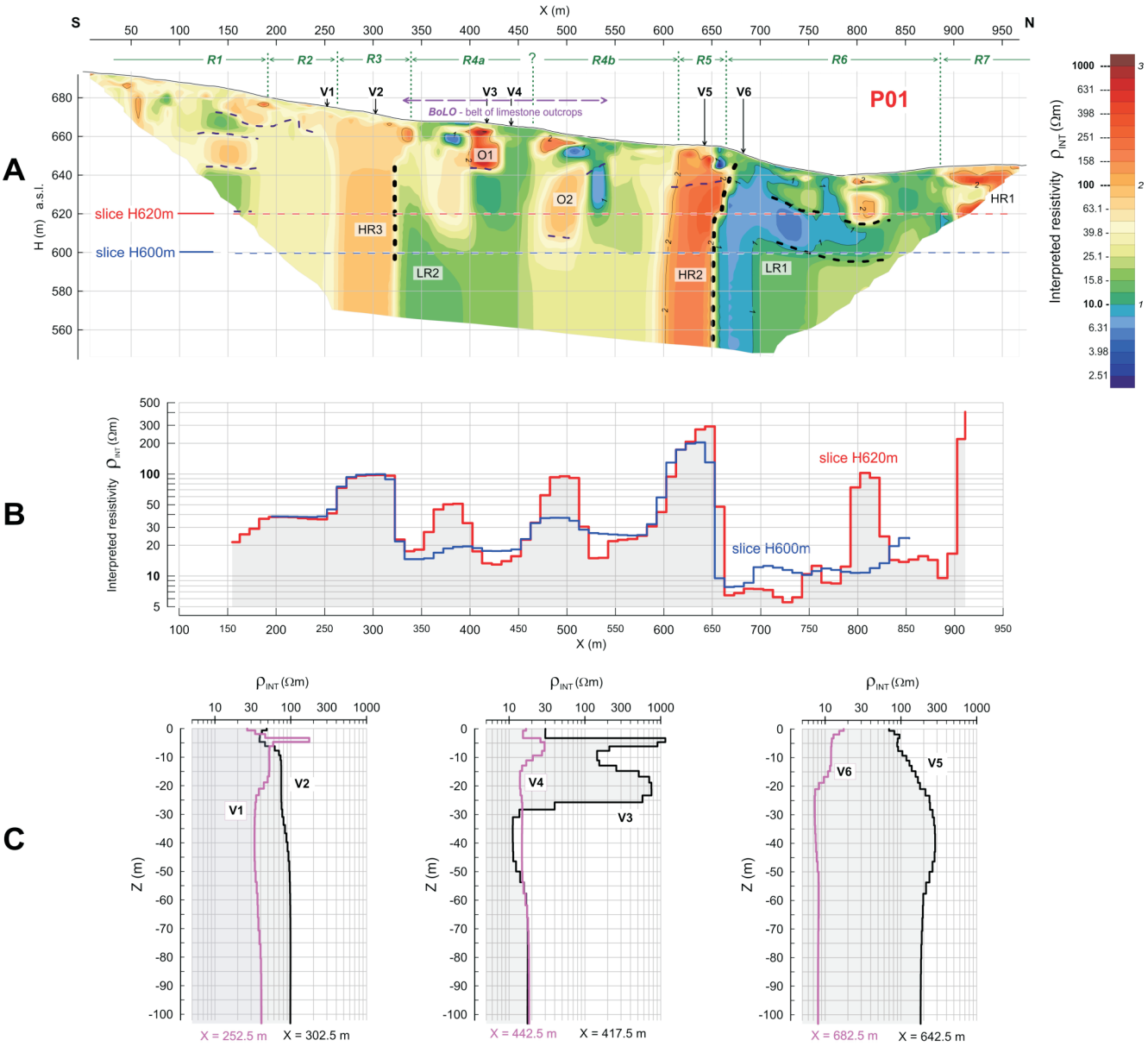

Fig. 5. P01 survey line; results of 2D inversion and analysis of the ERT data

A – inverse model resistivity section; R1–R7 – selected commented zones; HR1–HR3 – high-resistivity anomalies; LR1, LR2 – low-resistivity anomalies; O1, O2 – quasi-3D anomalies; V1–V6 – position of the vertical resistivity profiles extracted from the inversion model; slice H600m slice H620m– horizontal changes of the interpreted resistivity model at the indicated level; **B** – horizontal changes of the interpreted resistivity model at the level of 600 m a.s.l. and at the level of 620 m a.s.l.; **C** – vertical distribution of the interpreted resistivity (extracted from the inverse 2D model) for the indicated position (X) along the survey line

ERT FIELD DATA INVERSION RESULTS – GEOPHYSICAL ANALYSIS

The results for the initial ERT survey line P01 are shown in Figure 5. In the interpreted ERT section for the P01 profile (Fig. 5A), high-resistivity and low-resistivity zones of various forms (geometries) are distinguished. Notably, zones that are nearly vertical and deep-reaching are dominant in the cross-section (Fig. 5A, B). Such a style of resistivity distribution makes it possible to roughly distinguish zones in the study area that differ in the shape and range of resistivity anomalies. These zones are marked as R1, R2, …, R7. In the cross-section, black dotted lines are marked on the basis of the interpreted resistivity gradients (e.g., Mościcki et al., 2014; Woźniak and Bania, 2019a; Bania and Woźniak, 2022). These may indicate the presence of contacts (boundaries) in the geological medium.

In the cross-section (Fig. 5A) the most pronounced contact is between R5 and R6 zones. The R5 zone includes the HR2 high-resistivity anomalous object having the geometric shape of a "wall" and with a width of ~50 m. In this monolithic form, the interpreted electrical resistivity value varies in the range of 100 ~250 m. From the north, the HR2 anomaly very rapidly turns into a low-resistivity anomaly, LR1. The contact (marked with the nearly vertical thick dashed line noted earlier) is very sharp (Fig. 5B) and the transition is accompanied by a significant reduction in resistivity (there is a resistivity contrast of at least ~200:10, Fig. 5C – graph V6 *versus* V5). The resistivity in the LR1 anomaly drops <10 m in places. In its upper part (H >600 m a.s.l.), the LR1 anomaly changes into a more horizontal form, extending northwards. In this depth range, the HR2 "wall" is slightly tilted to the north. In part of the R6 zone, the distribution of the interpreted resistivity gradients (marked with dashed lines) suggests local layering of the geological medium. In the entire R6 zone, which is ~400 m wide, low resistivity values (<15 ~20 m) dominate. At the end of the cross-section, zone R7, the high resistivity HR1 anomaly reappears.

In the central part of the cross-section, zone R4 (Fig. 5A), local high-resistivity anomalies, O1 and O2, and other low-resistivity anomalies, are visible. The location of high-resistivity objects generally correlates with the discontinuous limestone rocks (parts of belt of limestone outcrops) visible at the surface. The low-resistivity medium may be related to the properties (dominance of the clayey component) of the medium in which the high-resistivity objects are embedded. Below the H level of ~600 m a.s.l., the geophysical structure is more homogeneous, but the resistivity is lower in the southern part, zone R4a (LR2), than in the northern part, zone R4b.

In the R3 zone (Fig. 5A), the HR3 high-resistivity anomaly is similar in form to the HR2 "wall". However, the resistivity here is clearly lower, ~ 60–100 m (Fig. 5C – compare plots V2 and V5). Below the altitude ~H = 620 m a.s.l., the contact between the HR3 and LR2 objects is clear, and the resistivity contrast here is ~80:15. On the southern side, the anomaly gently turns into a fairly homogeneous zone R2. The average resistivity here is ~40 m.

The last separate zone R1 may show, in its southern part (Fig. 5A), signs of a stratified medium, in the quasi-parallel distribution of the interpreted resistivity gradients. It is likely that the clearly visible belt of limestone outcrops (BoLO) is accompanied by buried objects. This is especially true for its northern border, which may coincide with the HR2 anomaly.

Figure 6 shows the inversion results for all ERT data. Profiles P03, P01, P02, P04 and P05 were parallel to P01, which made it possible to trace certain patterns in the subsurface geoelectrical structure of the BoLO and its surroundings. It can be seen that the HR2 anomaly dominates in P01, with its characteristic "wall" shape, and continues clearly in the P03, P02 and partially in the P04 cross-sections. Then it disappears and is not observed in the P05 section. On the northern side, the "wall" is adjoined by a low-resistivity zone, LR1, having local values clearly lower than 10 m. In the central part of the cross-sections analysed, ~350–550 m length, there are distinct anomalies of limited size, such as O1 and O2. Their shape changes from profile to profile. They quite clearly correlate with the individual and size-limited rocks that form the BoLO visible at the ground surface.

In the southern part of all cross-sections (Fig. 6), for around 300 m distance, significant high-resistivity HR3 anomalies were interpreted together with the accompanying low-resistivity LR2 anomalies on the northern side. Their shape (along the section line) is complicated and variable, not as regular as in the P01 profile.

In order to qualitatively estimate the longitudinal variability of the HR2 anomaly (Fig. 6), an ERT survey was performed along its axis on the P06 profile. The result of formal 2D inversion of the ERT data (Fig. 6, upper part, P06 cross-section) is strange: the HR2 anomaly is limited to shallow depth, and does not have a wall-like shape. This seems not to be real and is confusing, but such an effect of inversion may be explained and corroborated by analogue modeling, described later in the Discussion.

DISCUSSION

INTERPRETATION OF THE RESISTIVITY DATA

LITHOLOGICAL AND STRUCTURAL SUGGESTIONS: THE GEOPHYSICAL VIEWPOINT

The high-resistivity HR2 and HR3 objects (Fig. 5 – zones R3 and R5; Fig. 6), are most likely associated with the presence of limestone, while the low-resistivity LR1 and LR2 objects (Fig. 5 – zones R4a and R6; Fig. 6) may reflect a dominance of rocks rich in clayey material. Some of the high-resistivity objects, especially HR2, are evidently located outside the area of limestone occurrence at the ground surface (i.e., outside the BoLO). The upper parts (i.e., lying closer to the surface) of the HR1 and HR2 objects are slightly tilted towards the north, which is probably related to the direction of the tectonic forces that formed the PKB (nappes) in this area. A similar inference can be made by analysing the bends of the shape of the LR1 anomaly (Fig. 5A – zone R6) on parallel profiles (Fig. 6 – P03, P02, P04 and P05).

High-resistivity and size-limited zones observed in the central parts of the survey lines (such as O1 and O2; Fig. 6) are associated with invisible parts of the limestone rocks forming BoLO at the surface.

In the southern part of the research area (Fig. 5 – zone R2; Fig. 6), the geological medium is generally homogeneous as regards resistivity (~40 Ωm – mudstone?, clayey flysch?). However, certain horizontal zones may exist within these rocks (zone R1). On the northern side of the study area (Fig. 5 – zone R6 and Fig. 6) low-resistivity rocks predominate up to the depth of geoelectrical recognition. At the northern ends of the P01, P02, P04, and P05 cross-sections, a high-resistivity object HR1 appears, which perhaps may represent sandstone flysch.

Based on the analysis presented, it is possible to propose a probable model of the geological structure of the part of the PKB analysed. This is shown in Figure 7A using a digital elevation model image as the background map.

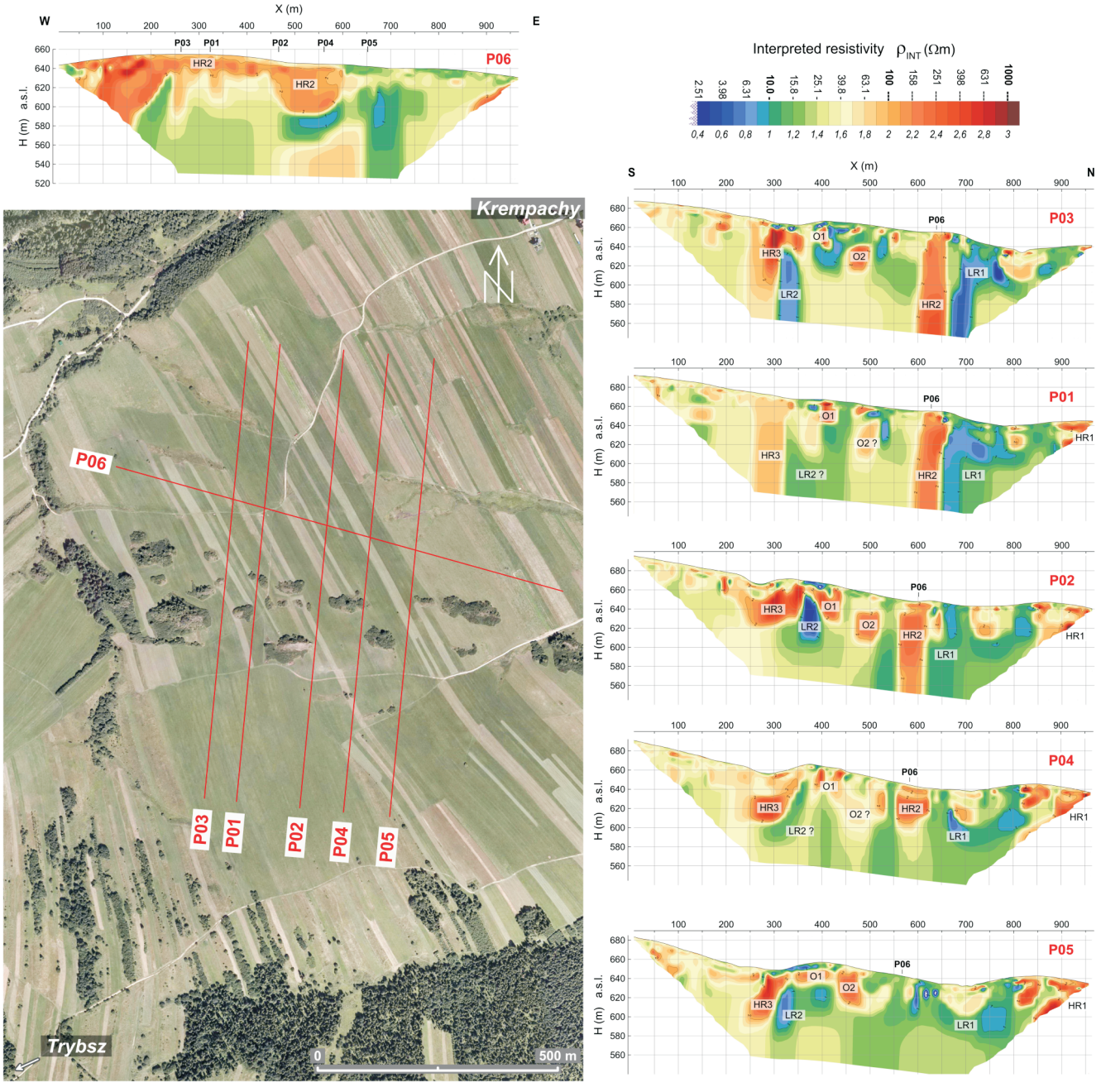

Fig. 6. Location of ERT profiles together with inverse model resistivity sections (source of orthophotomap: Google Earth)

For explanation see Figure 5

The geological structure has a zonal nature with a general WNW–ESE trend, as in the limestones constituting the BoLO visible at the surface (Fig. 7A).

In the N2 zone (Fig. 7A), rocks with resistivity greater than 100 Wm are present near the surface, which may be sandstone-dominated flysch. Farther south there is a relatively wide low-resistivity zone, N1, which may be considered as an area of shale and mudstone. In the central near-surface part of the N1 zone, there are units with more sandstones (50 ~100 m) reaching up to a depth of 20 m below the ground surface and characteristically curved (like a syncline). In the deeper parts of the N1 zone, signs of similar bending can be observed in clayey strata. The low-resistivity zone N1 is limited to the south by the most visible high-resistivity anomaly having the character of a kind of "wall" – zone B1. This form in its western part (P03, P01, and P02 cross-sections – Fig. 6) can reach a depth of at least 100 m; it breaks off abruptly on its eastern side (it is not registered in the section for the P05 profile). The azimuth of the "wall" strikingly coincides with the azimuth (~105°) of the Kramnica Mountain (Fig. 7A), which is a massive limestone outcrop located in the Przełom Białki Nature Reserve (Natura 2000) near Krempachy village. Perhaps the "wall" is an extension of it, hidden beneath the surface.

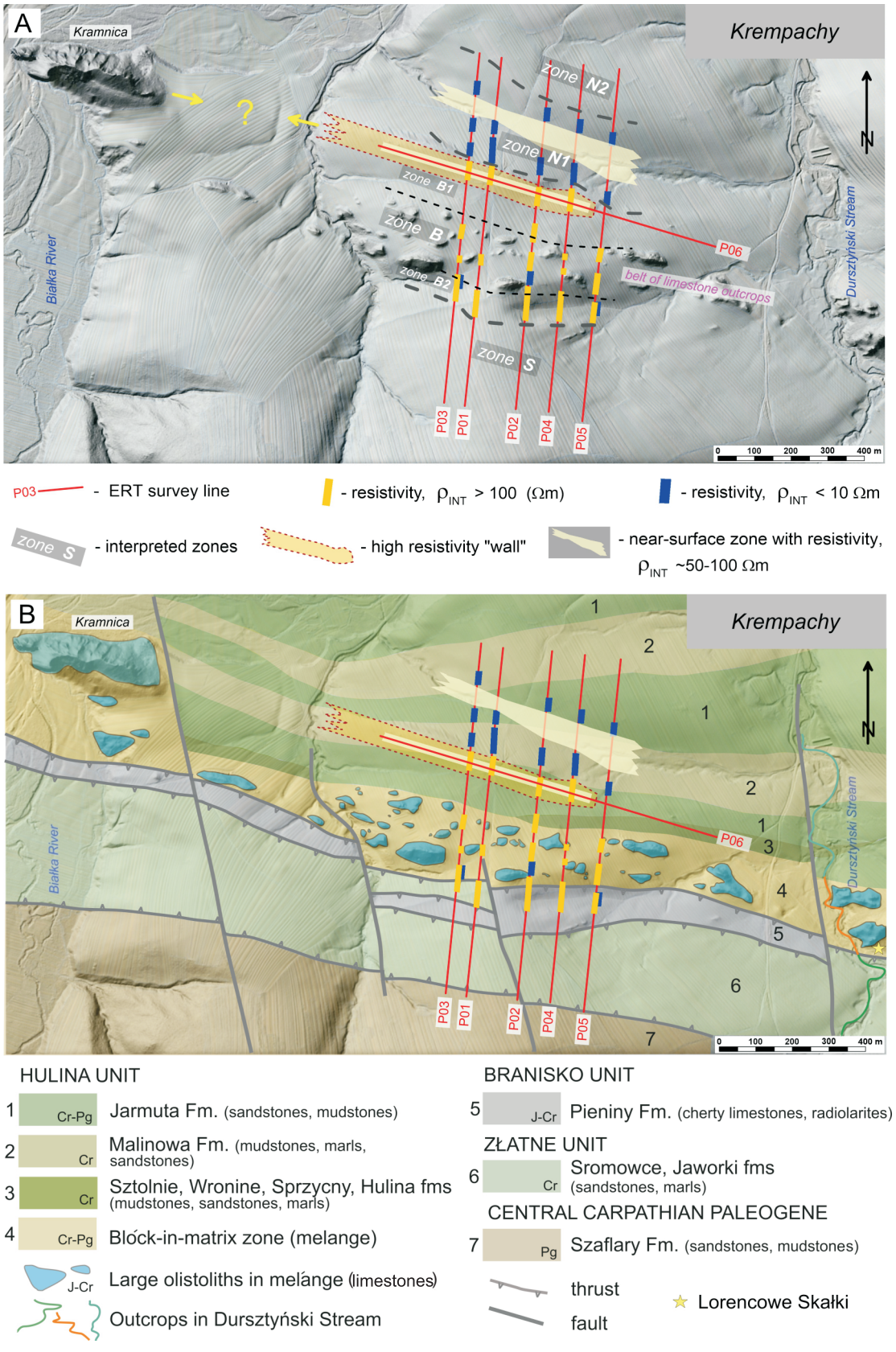

Fig. 7. Interpretation maps

A – ERT results – interpreted zones superimposed on the DEM image (with 1 m cell size; source: www.geoportal.gov.pl);
B – geological map with ERT zones superimposed (source of geological map: Cichostępski et al., 2024, modified)

In the south, apart from the BoLO rocks, there is zone B2 (Fig. 7A), in which outstanding high-resistivity anomalies appear in the sections for subsequent profiles P03, P01, P02, P04 and P05 (Fig. 6). It can be assumed that these rocks do not extend deeply, but rather are isolated limestone or sandstone blocks. They constitute an irregular belt. The shape (section) and size of the blocks varies and their depth range is limited to ~40–50 m.

On the southern side, in zone S (Fig. 7A), there are scarcely differentiated units with a resistivity of ~40 Ωm, most likely sandstone-dominated flysch. The situation here is clearly different from the conditions on the northern side of the BoLO, in the N1 zone, dominated by clayey strata.

The limestone rocks (outcrops) visible in the field (forming the BoLO) mostly have elongated shapes, and are clearly flattened, resembling vertical lenses. In most cases, these rocks are arranged roughly consistently, mostly according to the general course of the PKB (Fig. 7A).

GEOLOGICAL REMARKS WITH REFERENCE TO ROCKS FORMING THE PIENINY KLIPPEN BELT

The geological structure of the part of the PKB studied has zonal nature and a similar situation is observed in the ERT results. However, comparison of the maps (Fig. 7A, B) reveals both similarities and differences between the course of the geological boundaries (elaborated from geological studies) and the distribution of rock resistivity.

The central part is the belt of limestone outcrops that protrudes from the flysch matrix (Fig. 7). These are Jurassic-Early Cretaceous in age and were deposited on the Czorsztyn Ridge. The limestone rock visible at the surface is discontinuous and probably does not have deeper roots. Individual rocks (olistoliths?) are generally depth-limited, in most cases flattened, and arranged similarly, mostly following the PKB course. Locally, there are irregularities in the direction of elongation of these rocks, most likely of tectonic origin, representing transverse faults. However, the BoLO has invisible components that have been identified using the ERT survey results. The Upper Cretaceous-Paleogene flysch deposits crop in streams, especially in the Dursztyński Stream (also known as the Kręty Stream), east of the research area (Fig. 7B). The limestones are characterized by high resistivity (HR in Fig. 6) in contrast to the low resistivity (LR) of the surrounding flysch deposits. The lowest resistivity zone LR2 is especially visible in the ERT profiles P02, P03, and P05. This zone may correspond to the Upper Cretaceous red shales and marls cropping out in the Dursztyński Stream and in the area surrounding Lorencowe Skałki (Fig. 7B). The ERT survey allows the differentiation of several medium-sized olistoliths, such as O1 and O2, marked on the sections P01–P05 (Fig. 6). These olistoliths, as well as the surrounding marls, shales and flysch units, belong to zone B in Figure 7A.

The shape and arrangement of the BoLO rocks (Fig. 7) suggest (roughly simplifying) that they represent a block-in-matrix zone with olistoliths. The olistoliths represent the rocks of the Czorsztyn Succession (mainly crinoidal and nodular limestones) originally representing relatively brittle, continuous limestone layers. They slid down into the deep Magura Basin. They are surrounded by a matrix comprising mainly softer, more plastic rocks such as mudstones, marls and flysch. As a result of folding during orogeny (formation of nappes, etc.), this block-in-matrix zone became part of the Hulina Unit (Nappe) (Golonka et al., 2022), much later eroded to form the present outcrops.

The southern part (Fig. 7A – zone S) of the research area is dominated by scarcely differentiated units with a resistivity of ~40 Ωm and may represent the Branisko rock sequences. The southernmost part of zone S includes flysch deposits of, probably the Złatne Nappe and Central Carpathian Paleogene, similar to those exposed in the Dursztyński Stream (Fig. 7B). By contrast, the northern part of the research site is dominated by the low-resistivity (<10 Ωm) zone N1 (Fig. 7A), which may be considered as Upper Cretaceous variegated shales of the Malinowa Formation. The northernmost part of the research area (Fig. 7A – zone N2), where rocks with resistivity greater than 100 Ωm are present, may belong to the Upper Cretaceous-Paleocene Jarmuta Sandstone.

On the north side of the BoLO, the low-resistivity zone N1 (Fig. 7A) is limited to the south by the best-expressed high-resistivity anomaly (Fig. 6 – HR2) distinguished within zone B1 (Fig. 7A). The geological mapping indicate sandstones of the Jarmuta Formation. However, according to geophysical suggestions, this may be a hidden continuation of the well-known Kramnica olistolith (cf. Section: Lithological and structural suggestions: the geophysical viewpoint). On the southern side of the BoLO there are also invisible limestone rocks (Fig. 6 – HR3), but their forms are irregular and do not extend so deeply (Fig. 7A – zone B2).

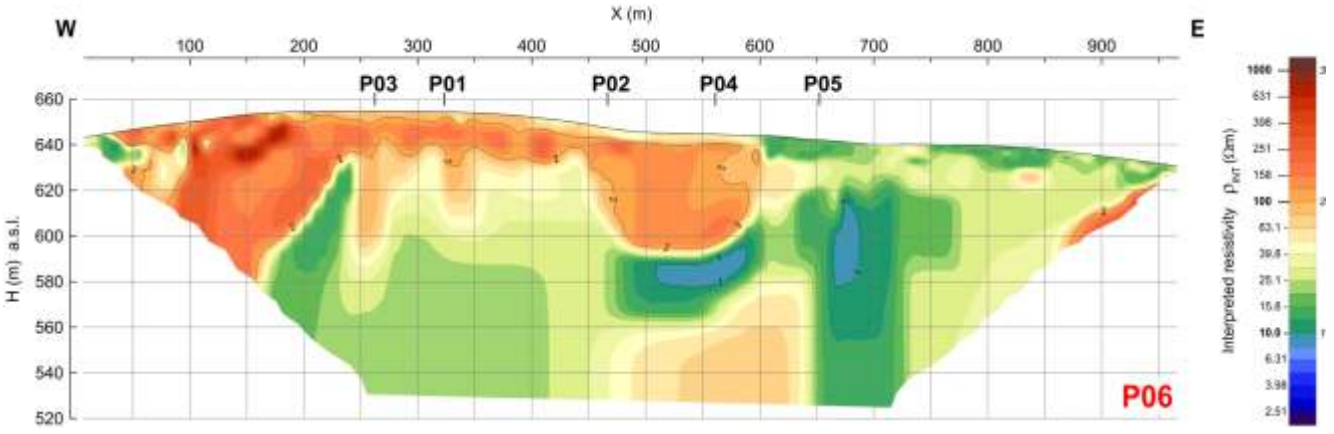

Fig. 8. Inversion of the ERT data for the P06 survey line

ANALYSIS OF THE P06 PROFILE RESULTS – NOTES ON THE CORRECT APPLICATION OF THE 2D ERT METHOD

As noted, the inversion results obtained for the P06 profile may be surprising (Figs. 5 and 7A).

The high-resistivity object visible in the P06 profile cross-section (Fig. 8) does not have the character of a "wall", as in the P01, P02, and P03 resistivity sections (Fig. 6), but rather takes the form of a high-resistivity "layer" lined with a zone of lower resistivity. Why so?

It may be easily explained by considering that the inversion *Res2Dinv* software (according to its purpose and principle of operation) forcibly adjusts the best 2D model to the measurement data. And yet the real situation – the course of the P06 profile in relation to the object (Fig. 7A) – is far from 2D! As a result, the electric current for a measurement array placed above a high resistivity "wall" along its longitudinal axis tends to "run away" into the environment where the resistivity is lower and current propagation is easier. The intensity of this phenomenon depends on the geometry of the system, the width of the "wall", and the resistivity contrast.

The correct 2D numerical inversion of ERT data depends on the degree to which the following assumptions are met:

- the survey line runs perpendicular to the geological structure, which is 2D. This means that each cross-section (profile) parallel to the one analysed should give identical results. However, it is obvious that in practice there are departures from this, as where a profile runs perpendicular to the outcrop or to the axis of the syncline/anticline/fault, an elongated structural form, etc;
- the terrain morphology is also 2D in relation to the survey line. However, in hilly or mountainous region, this is rarely the case.

Any deviation from these assumptions affects the result of the 2D inversion. Formally speaking, the geophysical model obtained from such an inversion is 2D (the distribution of interpreted resistivity as a cross-section of the 2D model in the XZ plane, where X is the distance along the survey line, and Z is the depth) and may not correspond well to the real, usually 3D, situation. Additionally, in a 2D inversion applied to a real 3D situation, the "interpreted" object visible in the cross-section may be an effect caused by the actual object lying outside the cross-section line (cf. e.g., Sjödahl et al., 2006; Dahlin et al., 2007; Bania and Ćwiklik, 2013). This is because (apart from the inadequate conditions for the 2D inversion) the electric field "spreads" throughout the space (Earth), "seeing" also what lies on both sides of the profile, not only under it.

To demonstrate the effect of a "false inversion" that actually occurred in the research on the P06 survey line, we performed appropriate numerical calculations (Fig. 9A) and physical modeling (Fig. 9B, C). A very simple geometrical model of a "wall" (Figs. 4D and 9B, C) immersed in a homogeneous medium was used. In numerical calculations, this was a perfect 2D situation, whereas the "wall" in physical modeling was spatially limited and had a 3D character. The assumed resistivity contrast in the numerical calculations was 10,000, and in the physical modeling it was infinite (the model of the "wall" was made of an insulator and immersed in water with a resistivity of ~30 Ωm). The arrangement of the measurement arrays was identical to that used in the field survey (only the dimensions were properly scaled down). Measurement data was subjected to *robust* inversion with an automatically adjusted grid size (the same settings as for field data inversion) using *Res2Dinv* software.

In numerical modeling, first, a 2D model of an appropriate size was built (Fig. 9A; NM-1). The dimensions of the "wall" were similar (geometrically proportional) to the field situation. The simulated measurement data were then calculated for the model and subjected to 2D inversion. In analogue modeling, the model of a finite (limited) "wall" was built of plastic plates (Figs. 4D and 9B, C; AM), maintaining dimensions similar to the numerical model NM-1. The right part of Figure 9 shows three cross-sections: the results of inversion.

The contour of the "wall", shown in the inversion sections (Fig. 9), is marked with a thin purple line. The colour scale gives the values of normalized resistivity A / N (A – anomaly, N – background, ambient resistivity; in the case of NM-1 it was 1 Ωm, and in the case of AM-1 and AM-2 it was the water resistivity).

As can be seen for the NM-1 model (Fig. 9A), the inversion result reflects very well the form, shape, and position of the high resistivity object. It is worse at recreating its real resistivity.

For the AM-1 and AM-2 models (Fig. 9B, C), the interpreted 2D cross-sections are completely different from the real model resistivity distribution. In addition, after the formal 2D inversion, zones with low resistivity (blue) appeared in the cross-sections. The resistivity here is more than two times lower than the background resistivity in the real model. When the situation is evaluated from the point of view of a physical phenomenon, it can be said that the electric current "escapes" from the thin layer of water covering the upper part of the high-resistivity "wall" and flows "sideways" in low-resistivity water. It definitely reduces the apparent resistivity measured. The phenomenon is exacerbated when the size of the measuring array is greater than the width of the "wall".

The general similarity of the modeled effect (Fig. 9) to the ERT results for the P06 profile (Fig. 8) is obvious.

CONCLUSIONS

ERT research has led to geological and geophysical conclusions, respectively concerning the structure of a part of the Pieniny Klippen Belt, and the specificity of the ERT application methodology.

The geological structure of the part of the PKB studied has a zonal nature that generally extends east-west (Fig. 7). Within the ERT inverse model resistivity sections, the high resistivity zones may be interpreted in terms of limestone and/or massive sandstone lithologies. In contrast, the low-resistivity zones correspond mainly to clay, marl and clay/shale strata. In the central part of the area analysed, a belt of limestone outcrops protrudes from the flysch matrix. Since limestones are characterized by much greater electrical resistivity than the matrix in which they are embedded, this allowed determination of their mutual spatial relationships by ERT. This sharp resistivity contrast enabled estimation of the size and depth range of several olistoliths.

In the area studied by ERT, there are three tectonic units (nappes): the southern Złatne Unit (flysch deposits), the central Branisko Unit (limestones and radiolarite deposits), and the northern Hulina Unit (northern part – siltstone, marl and sandstone deposits, southern part – limestone olistoliths in a flysch matrix). By comparing the geological map (Fig. 7B) with the results of the ERT research (Figs. 6 and 7A), it was found that there is only a partial correlation between the rock resistivity distribution and the presumed course of the boundaries of the tectonic units shown on the geological map, with some clear differences.

ERT turned out to be effective in recognition of the structural specificity of the part of the PKB analysed, though carefully lo-

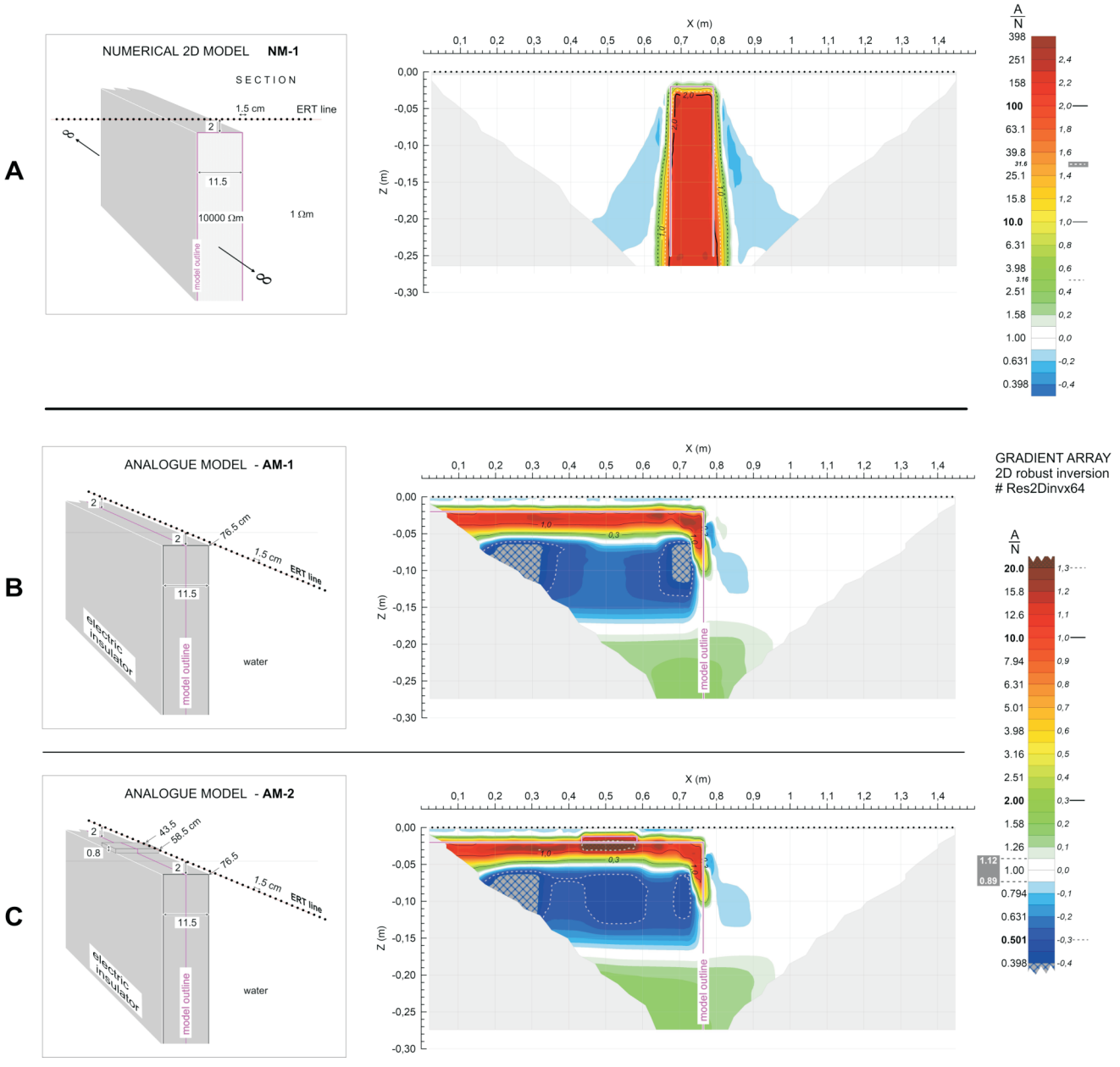

Fig. 9. Results of ERT modeling

A – numerical 2D model of the "wall", NM-1, and the result of 2D inversion; **B** – analogue model of a finite "wall" (3D object) with a flat-topped surface, AM-1, and the result of 2D inversion; **C** – analogue model of a finite "wall" (3D object) with locally raised top surface, AM-2, and the result of 2D inversion

cating the measurement lines was critical to reliable geophysical interpretation of the survey results.

We also analysed the basic conditions for the optimal use of ERT in the 2D mode. The orientation of the measurement line in relation to the expected geological structure is of fundamental importance and should be as perpendicular to the anticipated structure (assumed to be generally 2D) as possible. Otherwise, the results of 2D inversion of field data (even if the measurements are technically correct) may be misleading, in that the inverse model resistivity section obtained is inconsistent with the actual resistivity distribution. As a consequence, the geological conclusions may also be wrong. The issue has been demonstrated by performing appropriate numerical and analogue modeling that explains anomalous inversion results observed for some of the ERT field data.

Acknowledgements. The authors would like to thank T. Woźniak for minor text corrections. We benefited greatly from the constructive comments and suggestions of E. Jurewicz and two anonymous reviewers. This research was financially supported by the Polish National Science Centre grant NCN-2019/35/B/ST10/00241 and by the AGH University of Krakow subsidy funds no. 16.16.140.315.

REFERENCES

Akinbiyi, O.A., Oladunjoye, M.A., Sanuade, O.A., Oyedeji, O., 2019. Geophysical characterization and hydraulic properties of unconsolidated floodplain aquifer system in Wamako area, Sokoto State, north-western Nigeria. Applied Water Science, **9**: 177. https://doi.org/10.1007/s13201-019-1065-y

Andrusov, D., 1965. Geologie der tschechoslowakischen Karpaten. II. SAV, Akademie-Verlag, Bratislava, Berlin.

Antoniuk, J., Górecki, J., Mościcki, J., Szwed, E., 2005. Geofizyczne wspomaganie prac dokumentacyjnych na świętokrzyskich złożach kopalin ęglanowych (in Polish). Prace Naukowe Instytutu Górnictwa Politechniki Wrocławskiej, **109**: 3–12.

Bania, G., Ćwiklik, M., 2013. 2D Electrical Resistivity Tomography interpretation ambiguity – example of field studies supported with analogue and numerical modelling. Geology, Geophysics and Environment, **39**: 331–339. https://doi.org/10.7494/geol.2013.39.4.331

Bania, G., Woźniak, T., 2022. Subsurface imaging of fluvial deposits of the Wisła River valley in Kraków (southern Poland) by 2D ERT survey. Geological Quarterly, **66**: 23. https://doi.org/10.7306/gq.1655

Birkenmajer, K., 1961. Mapa geologiczna pienińskiego pasa skałkowego, skala 1:10.000, arkusz Dursztyn (in Polish). Instytut Geologiczny, Warszawa.

Birkenmajer, K., 1977. Jurassic and Cretaceous lithostratigraphic units of the Pieniny Klippen Belt, Carpathians, Poland. Studia Geologica Polonica, **45**: 1–158.

Birkenmajer, K., 1979. Przewodnik geologiczny po Pienińskim Pasie Skałkowym (in Polish). Wyd. Geol., Warszawa.

Birkenmajer, K., 2017. Geologia Pienin (in Polish). Monografie Pienińskie, **3**: 5–66..

Chambers, J.E., Wilkinson, P.B., Wardrop, D., Hameed, A., Hill, I., Jeffrey, C., Loke, M.H., Meldrum, P.I., Kuras, O., Cave, M., Gunn, D.A., 2012. Bedrock detection beneath river terrace deposits using three-dimensional electrical resistivity tomography. Geomorphology, **177–178**: 17–25. https://doi.org/10.1016/j.geomorph.2012.03.034

Cichostępski, K., Dec, J., Golonka, J., Waśkowska, A., 2024. Shallow seismic refraction tomography images from the Pieniny Klippen Belt (Southern Poland). Minerals, **14**: 155. https://doi.org/10.3390/min14020155

Csontos, L., Vörös, A., 2004. Mesozoic plate tectonic reconstruction of the Carpathian region. Palaeogeography, Palaeoclimatology, Palaeoecology, **210**: 1–56. https://doi.org/10.1016/j.palaeo.2004.02.033

Dahlin, T., 1996. 2D resistivity surveying for environmental and engineering applications. First Break, **14**: 275–283.

Dahlin, T., 2001. The development of electrical imaging techniques. Computers and Geosciences, **27**: 1019–1029. https://doi.org/10.1016/S0098-3004(00)00160-6

Dahlin, T., Zhou, B., 2004. A numerical comparison of 2D resistivity imaging with ten electrode arrays. Geophysical Prospecting, **52**: 379–398. https://doi.org/10.1111/j.1365-2478.2004.00423.x

Dahlin, T., Wisén, R., Zhang, D., 2007. 3D effects on 2D resistivity imaging – modelling and field surveying results. Near Surface 2007 – 13th EAGE European Meeting of Environmental and Engineering Geophysics, September 2007. https://doi.org/10.3997/2214-4609.20146558

Danielsen, B.E., Dahlin, T., 2010. Numerical modelling of resolution and sensitivity of ERT in horizontal boreholes. Journal of Applied Geophysics, **70**: 245–254. https://doi.org/10.1016/j.jappgeo.2010.01.005

Dortman, N.B., 1992. Petrophysics: reference. In: Three Books. Book One: Rocks and Minerals (in Russian). Nedra, Moscow.

Fox, R.C., Hohmann, G.W., Killpack, T.J., Rijo, L., 1980. Topographic effects in resistivity and induced polarization surveys. Geophysics, **45**: 75–93. https://doi.org/10.1190/1.1441041

Golonka, J., Krobicki, M., 2007. Dunajec River rafting as one of the most important geotouristic object of the future trans-bordering PIENINY Geopark. Geoturystyka. Geotourism, **3**: 29–44.

Golonka, J., Krobicki, M., Waśkowska, A., Cieszkowski, M., Ślączka, A., 2015. Olistostromes of the Pieniny Klippen Belt, Northern Carpathians. Geological Magazine, **152**: 269–286. https://doi.org/10.1017/S0016756814000211

Golonka, J., Pietsch, K., Marzec, P., 2018. The North European Platform suture zone in Poland. Geology, Geophysics and Environment, **44**: 5–16. https://doi.org/10.7494/geol.2018.44.1.5

Golonka, J., Pietsch, K., Marzec, P., Kasperska, M., Dec, J., Cichostępski, K., Lasocki, S., 2019. Deep structure of the Pieniny Klippen Belt in Poland. Swiss Journal of Geosciences, **112**: 475–506. https://doi.org/10.1007/s00015-019-00345-2

Golonka, J., Waśkowska, A., Cichostępski, K., Dec, J., Pietsch, K., Łój, M., Bania, G., Mościcki, W.J., Porzucek, S., 2022. Mélange, flysch and cliffs in the Pieniny Klippen Belt (Poland): An overview. Minerals, **12***:* 1149. https://doi.org/10.3390/min12091149

Hellman, K., Johansson, S., Olsson, P., Dahlin, T., 2016. Resistivity inversion software comparison. 22nd European Meeting of Environmental and Engineering Geophysics, Near Surface Geoscience 2016. https://doi.org/10.3997/2214-4609.201602016

Hirsch, M., Bentley, L.R., Dietrich, P., 2008. A comparison of electrical resistivity, ground penetrating radar and seismic refraction results at a river terrace site. Journal of Environmental and Engineering Geophysics, **13**: 325–333. https://doi.org/10.2113/JEEG13.4.325

Hojat, A., Ferrario, M., Arosio, D., Brunero, M., Ivanov, V.I., Longoni, L., Madaschi, A., Papini, M., Tresoldi, G., Zanzi, L., 2021. Laboratory studies using electrical resistivity tomography and fiber optic techniques to detect seepage zones in river embankments. Geosciences, **11**: 69. https://doi.org/10.3390/geosciences11020069

Ikhane, P.R., Omosanya, K.O., Akinmosin, A.A., Odugbesan, A.B., 2012. Electrical Resistivity Imaging (ERI) of slope deposits and structures in some parts of Eastern Dahomey Basin. Journal of Applied Sciences, **12**: 716–726. https://doi.org/10.3923/jas.2012.716.726

Kabanikhin, S., Tikhonov, N., Ivanov, V., Lavrentiev, M., 2008. Definitions and examples of inverse and ill-posed problems. Journal of Inverse and Ill-posed Problems, **16**: 317–357.

Keller, G.V., Frischknecht, F.C., 1966. Electrical Methods in Geophysical Prospecting. Pergamon Press, Oxford, New York. International Series of Monographs in Electromagnetic Waves, **10**.

Kobranova, V.N., 1989. Petrophysics. Mir Publishers, Springer, Moscow, Berlin.

Kondracki, J., 2001. Geografia Regionalna Polski (in Polish). PWN, Warsaw.

Książkiewicz, M., 1977. Tectonics of the Carpathians. In: Geology of Poland, **4**, Tectonics (ed. W. Pożaryski): 476–604. Wyd. Geol., Warszawa.

Loke, M.H., 2000. Topographic modelling in resistivity imaging inversion. 62nd EAGE Conference and Technical Exhibition Extended Abstracts, D-2. http://www.geotomosoft.com/topoabs.pdf

Loke, M.H., 2012. Tutorial: 2-D and 3-D Electrical Imaging Surveys. Geotomo Software, Malaysia. http://refhub.elsevier.com/S0926-9851(18)31023-1/rf0365

Loke, M.H., Ackworth, I., Dahlin, T., 2003. A comparison of smooth and blocky inversion methods in 2D electrical imaging surveys. Exploration Geophysics, **34**: 182–187. https://doi.org/10.1071/EG03182

Loke, M.H., Chambers, J.E., Rucher, D.F., Kuras, O., Wilkinson, P.B., 2013. Recent developments in the direct-current geoelectrical imaging method. Journal of Applied Geophysics, **95**: 135–156. https://doi.org/10.1016/j.jappgeo.2013.02.017

Lu, D.B., Zhou, Q.Y., Junejo, S.A., Xiao, A.L., 2015. A systematic study of topography effect of ERT based on 3-D modeling and inversion. Pure and Applied Geophysics, **172**: 1531–1546. https://doi.org/10.1007/s00024-014-1015-4

Ludwiniak, M., 2010. Multi-stage development of the joint network in the flysch rocks of western Podhale (Inner Western Carpathians, Poland). Acta Geologica Polonica, **60**: 283–316.

McNeill, D.J., 1980. Electrical Conductivity of Soils and Rocks. Geonics Limited, Technical Note TN-5, Ontario, Canada.

Metwaly, M., AlFouzan, F., 2013. Application of 2-D geoelectrical resistivity tomography for subsurface cavity detection in the eastern part of Saudi Arabia. Geoscience Frontiers, **4**: 469–476. https://doi.org/10.1016/j.gsf.2012.12.005

Mościcki, W.J., 2008. 2D resistivity imaging of an anisotropic 3D body – results of a laboratory experiment. Near Surface 2008, 14th European, Meeting of Environmental and Engineering Geophysics, 15–17 September 2008, Kraków, Poland. EAGE 2008, Extended Abstracts and Exhibitors' Catalogue, P23.

Mościcki, W.J., Bania, G., Ćwiklik, M., Borecka, A., 2014. DC resistivity studies of shallow geology in the vicinity of Vistula River flood bank in Czernichów village (near Krakow in Poland). Studia Geotechnica et Mechanica, **36**: 63–70. https://doi.org/10.2478/sgem-2014-0008

Neumayr, M., 1871. Jurastudien. Der penninische Klippenzug. Jahrbuch der Kaiserlich-Königlichen Geologischen Reichanstalt, **21**: 451–536.

Nur Amalina, M.K.A., Nordiana, M.M., Bery, A.A., Bin Anuar, M.N.A., Maslinda, U., Sulaiman, N., Saharudin, M.A., Hisham, H., Nordiana, A.N., Taqiuddin, Z.M., 2017. Application of 2-D resistivity imaging and seismic refraction method in identifying the structural geological contact of sedimentary lithologies. IOP Conference Series: Earth and Environmental Science, **62**: 012005. https://doi.org/10.1088/1755-1315/62/1/012005

Plašienka, D., Aubrecht, R., Bezák, V., Bielik, M., Broska, I., Bučová, J., Fekete, K., Gaži, P., Gedl, P., Golej, M., Halásová, E., Hók, J., Hrdlička, M., Jamrich, M., Józsa, Š., Klanica, R., Konečný, P., Kubiš M., Madarás, J., Majcin, D., Marko, F., Molčan Matejová, M., Potočný, T., Schlögl, J., Soták, J., Suan, G., Šamajová, L., Šimonová, V., Teťák, F., Vozár, J., 2021. Structure, composition and tectonic evolution of the Pieniny Klippen Belt – Central Western Carpathian contiguous zone (Kysuce and Orava regions, NW Slovakia). Comenius University Bratislava, 148.

Sikora, W., 1971. Esquisse de la tectogénèse de la zone des Klippes des Pieniny en Pologne d'après de nouvelles données géologiques. Rocznik Polskiego Towarzystwa Geologicznego, **41**: 221–239.

Šilhán, K., Pánek, T., 2010. Fossil and recent debris flows in medium–high mountains (Moravskoslezské Beskydy Mts., Czech Republic). Geomorphology, **124**: 238–249. https://doi.org/10.1016/j.geomorph.2010.03.026

Sjödahl, P., Dahlin, T., Zhou, B., 2006. 2.5D resistivity modeling of embankment dams to assess influence from geometry and material properties. Geophysics, **71**: G107–G114. https://doi.org/10.1190/1.2198217

Szalai, S., Szokoli, K., Pracser, E., Metwaly, M., Zubair, M., Szarka, L., 2020. An alternative way in electrical resistivity prospection: the quasi-null arrays. Geophysical Journal International, **220**: 1463-1480. https://doi.org/10.1093/gji/ggz518

Telford, W.M., Geldart, L.P., Sheriff, R.E., 1990. Applied Geophysics. Cambridge University Press.

Watycha, L., 1964. Szczegółowa Mapa Geologiczna Polski 1:50.000 (bez utworów czwartorzędowych). Rejon Karpat i Przedgórza, arkusz Nowy Targ (in Polish). Wyd. Geol., Warszawa.

Watycha, L., 1975. Szczegółowa Mapa Geologiczna Polski 1:50 000, arkusz Nowy Targ (in Polish). Wyd. Geol., Warszawa.

Woźniak, T., Bania, G., 2019a. Analysis of the tectonic and sedimentary features of the southern margin of the Krzeszowice Graben in Southern Poland based on an integrated geoelectrical and geological studies. Journal of Applied Geophysics, **165**: 60–76. https://doi.org/10.1016/j.jappgeo.2019.04.010

Woźniak, T., Bania, G., 2019b. Integrated geoelectrical and geological data sets for shallow structure characterization of the southern margin of the Krzeszowice Graben (Southern Poland). Data in Brief, **25**: 104157. https://doi.org/10.1016/j.dib.2019.104157

Woźniak, T., Bania, G., Mościcki, J.W., Ćwiklik, M., 2018. Electrical resistivity tomography (ERT) and sedimentological analysis applied to investigation of Upper Jurassic limestones from the Krzeszowice Graben (Kraków Upland, southern Poland). Geological Quarterly, **62**: 287–302. https://doi.org/10.7306/gq.1403